Chapter 2
Materials and Characterization Techniques

Abstract This chapter reviews characterization techniques with emphasis on their introduction and principle of operation for the experiments to achieve the goal of this thesis. Lights scattering techniques like dynamic light scattering, static light scattering, depolarized light scattering; deformation technique like rheology, microscopic technique such as transmission electron microscopy were used to probe the samples. Other techniques such as Raman spectroscopy, viscometry and tensiometry were also used. In addition, we also give brief accounts of materials such as clays and their characterization and solvents used in this thesis work.

2.1 Materials Used

2.1.1 Nanoclays

Laponite RD and *Na* Montmorillonite (Cloisite *Na*) were purchased from Southern Clay products, USA and used as received. Sample preparation is described in respective chapters.

2.1.2 Solvents

Triple de-ionized water was purchased from Praveen Scientific, India. Organic solvents: methanol (MOH), ethanol (EOH), 1-propanol (POH), hexanol and octanol were purchased from Merck. The pH adjustments were done using 0.1N NaOH and 0.1N HCl obtained from Fisher Scientific, India. All solvents were of spectroscopic grade and used as received.

R. K. Pujala, *Dispersion Stability, Microstructure and Phase Transition of Anisotropic Nanodiscs*, Springer Theses, DOI: 10.1007/978-3-319-04555-9_2,

2.2 Characterization Techniques

2.2.1 Laser Light Scattering

Light scattering is a non-invasive technique for characterizing macromolecules and a wide range of particles in solution. In contrast to most methods of characterization, it does not require external calibration standards. In this sense, it is an absolute technique. Scattering is a very powerful technique to study the physical properties (structure and dynamics) of a system and is used routinely for measuring the hydrodynamic size of colloids and nanoparticles, particularly in dispersions. Scattering results from the interaction of the electrons in the molecules with oscillating electric field of radiation. Thus, a dipole is induced in the molecules, which oscillate with the electric field. Since an oscillating dipole is a source of electromagnetic radiation, the molecules emit light, called scattered light. The difference in energy between the incident and scattered radiation determines the nature of scattering whether the phenomena is elastic (Rayleigh scattering), quasi-elastic scattering (Rayleigh-Brillouin scattering) or inelastic scattering (Raman scattering). The technique of light scattering has an advantage of being non-invasive probe method provided the intensity is not high enough to ionize the system. To probe a wide range of length scale, different scattering mechanisms are used i.e. typical length scale accessible in light scattering is up to 1,000 nm whereas in the case of neutron scattering it is up to 100 nm, X-ray scattering can probe up to 100 nm and for probe length scale smaller than this, one has to go for electron scattering.

(i) **Dynamic Light Scattering**

Dynamic light scattering (DLS) probes the transport properties like diffusion coefficient which in turn determines the hydrodynamic radius of the nanoparticles, macromolecules etc. in liquid environments. In a light scattering experiment a monochromatic beam of laser light impinges on a sample and is scattered into a detector placed at an angle θ with respect to the transmitted beam. The intersection between the incident and scattered beams defines a volume V, called the scattering or illuminated volume [3]. Dynamic light scattering [4–8] is sensitive to the diffusion of scattering particles in solution, as it measures the intensity of light scattered at a fixed angle, which is then analyzed with an autocorrelator. The resulting correlation function has the particle diffusion coefficient as one of its arguments, which can be used to calculate the hydrodynamic radius of the particle through Stoke-Einstein relation.

In our work, dynamic laser light scattering experiments were performed on digital correlator (PhotoCor Instruments, USA) and a homemade goniometer that was operated in the multi-tau mode (logarithmically spaced channels). The time scale spanned 8-decades, i.e. from 0.5 μs to 10 s. The samples were loaded into 5 ml cylindrical borosilicate glass cells and sealed. These cells were housed inside a thermostated bath (scattering geometry), and the temperature was regulated by a PID temperature controller to an accuracy of ±0.1 °C. The excitation source was a He-Ne laser emitting at a wavelength of 632.8 nm in linearly polarized single frequency mode, which was

focused on the sample cell and scattered light was detected by a photo-multiplier tube (Hamamatsu), and the signal was converted into intensity auto-correlation function by a digital correlator. The scattering angle was fixed at 90° and the measured intensity auto-correlation functions were analyzed by the CONTIN regression software after ensuring that the relaxation time distribution function did not contain more than one distribution. Robustness of the DLS results was decided based on two criteria: sample to sample accuracy, and data reproducibility within the same sample. In all the experiments, the difference between the measured and calculated base line was not allowed to go beyond ±0.1 %. The data that showed excessive baseline difference were rejected.

In a typical DLS experiment, we measured the time correlation function $g_2(t)$ of the scattered intensity $I(t)$ at a given q (scattering wave vector) defined by Berne et al. [4]

$$g_2(t) = \frac{\langle I(t')\ I(t'+t)\rangle}{\langle I(t')\rangle^2} \tag{2.1}$$

where $q = (4\pi n/\lambda)\ \sin(\theta/2)$, n is the refractive index of the solution, θ is the scattering angle, and λ is the wavelength of light. The intensity correlation function $g_2(t)$ is related to the scattered field auto-correlation function, $g_1(t)$ through the Siegert relation [4–8]

$$g_2(t) = A + B|g_1(t)|^2 \tag{2.2}$$

where A defines the baseline of the correlation function as,

$$|g_2(t)|_{t\to\infty} = A \tag{2.3}$$

and B is the spatial coherence factor. The ratio (B/A) is the signal modulation and better data quality demands $(B/A) \geq 50$ %. For solutions containing particles undergoing Brownian motion (i.e., polymer or colloidal solutions), the field auto-correlation function, $g_1(t)$ is given as,

$$g_1(t) = \sum_i \mathrm{A_i} \exp\left(-\Gamma_i \mathrm{t}\right) \tag{2.4}$$

where Γ_i is the relaxation frequency, which characterizes various relaxation modes that include relaxations due to the translational diffusion, rotational diffusion and bending modes etc. The relative mode strength (amplitude) of the ith relaxation mode is A_i. For the present case, center of mass diffusion is the dominant process and Γ_i has been identified as $\Gamma_i = D_i\ q^2$. Here the translational diffusion coefficient of the ith particle is D_i. The expression for $g_1(t)$ remains valid for polydisperse samples, and for situation where the relaxation frequency distribution has several peaks. Polydispersity P can be defined as,

$$P = \frac{\left\langle (D - \overline{D})^2 \right\rangle}{(\overline{D})^2} \tag{2.5}$$

Further details about DLS can be found elsewhere [4, 8]. According to Einstein relation, the $\bar{D}_o$(the z-average diffusion coefficient at infinite dilution) is inversely proportional to the translational frictional coefficient, f_t at infinite dilution given by the relation,

$$\bar{D}_o = \frac{k_B T}{f_t} \tag{2.6}$$

where k_B is Boltzmann constant and T is absolute temperature. The value of f_t obtained via Eq. 2.6 can be used for a direct estimation of hydrodynamic radius, R_h of the particles provided they have a spherical shape using the relation $f_t = 6\pi\eta R_h$ as per the Stokes law. Further one can write

$$D = \frac{k_B T}{6\pi\eta R_h} \tag{2.7}$$

where η is the solvent viscosity at temperature T. The intensity correlation function is related to diffusion coefficient of the particles and hence to the hydrodynamic radius by Stoke-Einstein equation through Eq. 2.7.

(ii) **Analysis of Non-ergodic Samples**

The aging behaviour and slow dynamics is best probed by dynamic light scattering experiments. The intensity auto-correlation function $g_2(q,t)$ cannot be correlated directly to the corresponding dynamic structure factor $g_1(q,t)$ via the Siegert relation $g_2(q,t) = A + B|g_1(q,t)|^2$, where A defines the baseline of the correlation function as $|g_2(t)|_{t\to\infty} = A$, and B is the spatial coherence factor. Complications are caused when the scattering centers in the dispersion phase are localized near fixed mean positions and are able only to execute limited Brownian motion about the same. Here the system is considered to be arrested. A completely ergodic system is one where the time and the ensemble averages are identical, and the system is stationary implying that the process is independent of the origin of time which is adequately satisfied only in case of scattering from homogeneous dilute solutions. The non-ergodicity problem in DLS measurements has been dealt with in several ways which include rotating the sample to probe the entire phase space, expanding the incident beam to increasing the scattering volume and extracting the non-ergodic contribution from the measured data as a heterodyne contribution.

Herein, we address the problem in the following way. The normalized intensity correlation function, $g_2(q, t)$, obtained from the sample in arrested phase can be related to the dynamic structure factor, $g_1(q, t)$ as [9]

$$g_2(q,t) = 1 + \beta'\left[2X(1-X)g_1(q,t) + X^2|g_1(q,t)|^2\right] \tag{2.8}$$

where β' is the coherence factor having a maximum value of 1. In a real experiment it defines the signal modulation which is a measure of the signal-to-noise ratio in the data. The parameter X ($0 \le X \le 1$) defines the ergodicity via the amount of heterodyne contribution present in the correlation $g_2(q, t)$ data. When the value of $X = 1$, the system is completely ergodic i.e., in the sol state and the

Siegert relation is established; however in the arrested state $X < 1$ and the term $2X(1 - X)$ makes a finite contribution to $g_2(q, t)$ and hence it must be accounted for. The intercept of the plot of $[g_2(q, t) - 1]$ versus delay time t at $t \to 0$ gives β' $[2X - X^2]$ from which the value of X can be calculated if β' is known, which is an instrumental factor. The measured intensity auto-correlation data was analyzed exactly following the description given elsewhere [9]. The pre-factor of the linear term in $g_1(q, t)$ in Eq. 2.8 is much larger than the quadratic second term. Thus

$$g_1(q,t) \approx \left[g_2(q,t) - 1\right] / \left[2\beta'(X(1-X))\right] \tag{2.9}$$

The values of the heterodyne parameter X is always less than 1 except in the homogeneous dilute solutions where ergodicity is expected. The exact evaluation of the dynamic structure factor $g_1(q, t)$ from the measured intensity auto-correlation function $g_2(q, t)$ was achieved by putting the values of β' and X into Eq. 2.9 and hence the non-ergodic contribution was removed.

(iii) **Static Light Scattering**

In static light scattering solute particles are taken as stationary. Intensity of the scattered light adjusted for background scattering and normalized to reference solvent gives the Rayleigh ratio $R_s(q)$ which can be expressed for dilute solution as [5–8]

$$\left(\frac{1}{R_s(q)}\right)\left(\frac{4\pi^2 n^2 (dn/dc)^2}{N_A \lambda^4}\right) = \frac{1}{P(q)M_w} + 2Bc \tag{2.10}$$

where c is concentration of macromolecule, N_A is Avagadro's number, M_w is the weight averaged molecular weight of macromolecule in solution, B is the second virial coefficient describing interparticle interactions in solution and $P(q)$ is a particle shape factor. If a particle size is small compared to light wavelength, then it obviously acts as point scatterer, and its shape is irrelevant for scattering i.e. $P(q) = 1$. When the particle size becomes comparable to the wavelength used in the experiment $P(q)$ can be approximated reasonably well as a quadratic function of qR_g and the scattering profiles can be used to determine the particle radius of gyration. For random coil in very low scattering angle limit (Guinier region), $P(q)$ is given by,

$$P(q) = 1 - \frac{q^2 R_g^2}{3}; Rg < q^{-1} \tag{2.11}$$

The static structure factor is the Fourier transform of the pair correlation function which in turn is the probability of finding of a particle at r, given that a particle is present at the origin. Figure 2.1 shows the schematic of the Light scattering set up used in my work for static and dynamic measurements. It comprises of a 35 mW He–Ne Laser radiating at 632.8 nm digital correlator (PhotoCor instrument, USA) that was operated in the multi-tau mode (logarithmically spaced channels). The time scale spanned 8-decades, i.e. from 0.5 μs to 10 s. The samples were loaded into cylindrical borosilicate glass cells and sealed. These cells were housed inside

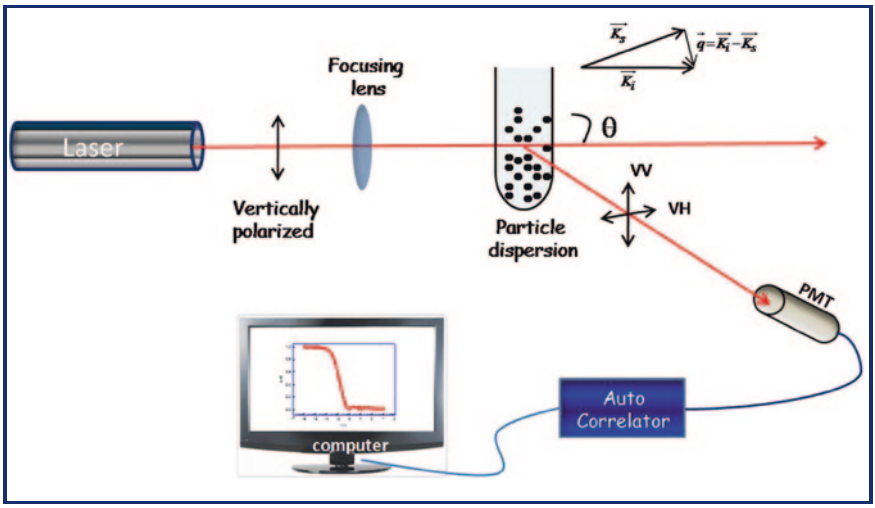

Fig. 2.1 Schematics of light scattering set up

a thermostated bath (scattering geometry) and temperature was regulated by a PID temperature controller to an accuracy of ±0.1 °C. The measured intensity auto-correlation function was analyzed by the CONTIN regression software.

(iv) **Depolarized Light Scattering**

The geometrical anisotropy of the scattering particles depolarizes the incident light, and the scattered electrical field can be decomposed into the parallel E_{VV} *(q, t)*, and perpendicular E_{VH} *(q, t)* components, with respect to the direction of the incident polarization. These quantities fluctuate due to the random translational and rotational motion of the particles, and one can define two distinct dynamic structure factors or electric field correlation functions using these components of the scattered field. A block diagram for the depolarized light scattering is shown in Fig. 2.2. The analyzer was kept at right angle to the direction of the propagation of the laser light so as to minimize the effect of the stray light and the presence of an interference filter ensured that signal to noise ratio was robust. The angle in the analyzer was adjusted either to 0 or 90° respectively as per the requirement. The zero degree alignment of the analyzer meant that only the parallel component (I_{VV}) of the scattered light passed through it to the detector whereas the 90° alignment of the analyzer ensured passage of only perpendicular component (I_{VH}) of the scattered light.

2.2.2 Rheology

Colloidal systems can be viscoelastic, that is, they can show both solid and fluid like characteristics. The solid like response of the system is set by its elasticity

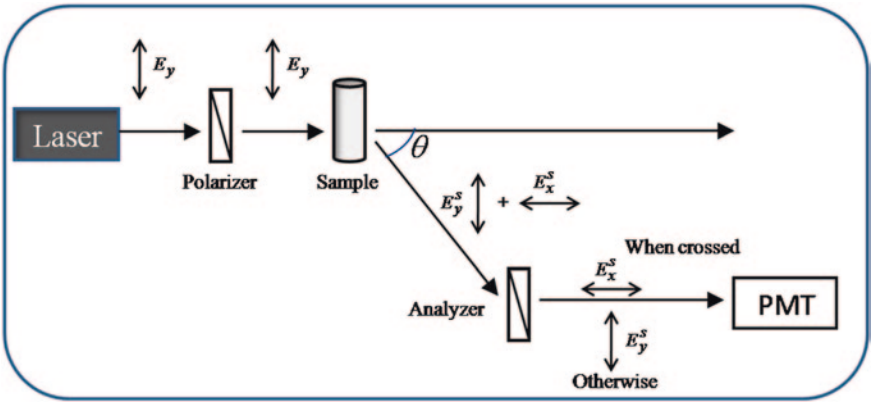

Fig. 2.2 Block diagram for depolarized light scattering

and the fluid like response by its viscosity. We can measure the material properties of the systems by means of rheometer. Rheology is the study of flow and deformation of matter. In practice, Rheology is principally concerned with extending the "classical" disciplines of elasticity and fluid mechanics (Newtonian) to materials whose mechanical behavior cannot be described with classical theories [7]. It is also concerned with establishing predictions for mechanical behavior (on the continuum mechanical scale) based on the micro or nanostructures of the materials. Rheology unites the seemingly unrelated fields of plasticity and non-Newtonian fluids by recognizing that both these types of materials are unable to support a shear stress in static equilibrium. In this sense, a plastic solid is a fluid. One of the tasks of rheology is to empirically establish the relationship between deformation and stress and their derivatives by adequate measurements. Such relationships are then amenable to mathematical treatment by the established methods of continuum mechanics.

There are two common approaches used in rotational Rheometer, controlled shear rate and controlled stress. In the controlled shear rate approach, the material being studied is placed between two plates. One of the plates is rotated at a fixed speed and the torsional force produced at the other plate is measured. Hence, speed (strain rate) is the independent variable and torque (stress) is the dependent variable. In the controlled stress approach, the situation is reversed. A torque (stress) is applied to one plate and the displacement or rotational speed (strain rate) of that same plate is measured. This latter approach (controlled stress) is better for determining apparent yield stress because the variable of primary interest can be more carefully controlled. That is, in the controlled stress approach it is possible to gradually increase the stress applied to the material and detect the point at which yield first occurs. Conversely, in the controlled rate approach, yielding actually has to be occurring before measurement can even occur. Hence, apparent yield stress can only be measured by back extrapolation from a finite level of motion to the point of zero motion [2].

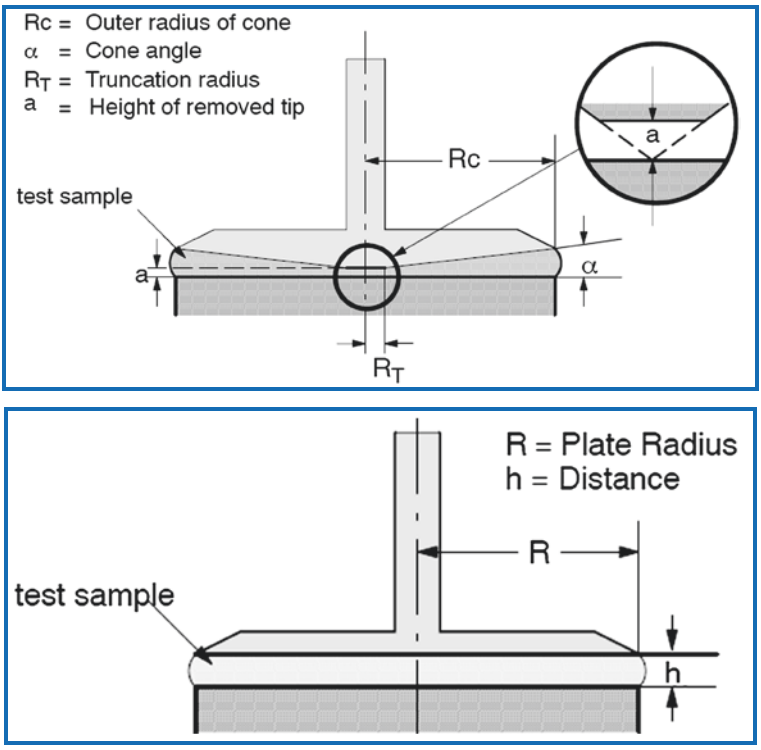

Fig. 2.3 Schematic of cone-plate and plate-plate geometry

The controlled stress approach provides three alternative experimental methods for determining apparent yield stress: (1) Stress can be ramped slowly from zero to some higher value. The stress level at which motion first occurs is the apparent yield stress. As indicated previously, this value may be affected by the stress ramp rate (rate of stress increase). (2) After initially shearing the material at a stress above the yield stress, the stress can be decreased in a slow ramp and the point where motion stops is the apparent yield point. Again as indicated previously, this value may be affected by the decreasing ramp rate and the time-dependent ability of the material to rebuild structure. (3) A creep experiment can be used where stress is applied to the material and strain (displacement) is monitored with time to establish an equilibrium yield stress.

The rheology experiments were performed using an AR-500 stress controlled rheometer (T.A. Instruments, UK). Different geometries used for rheological studies include the stainless steel cone plate geometry (diameter 20 mm and angle 20°) and parallel plate geometry (diameter 20 mm). The cone plate and parallel plate geometries are shown in Fig. 2.3. Rheological studies were carried out in different mode whose details are as follows:

2.2.2.1 Modes of Operation

(a) **Flow Mode**

In flow mode, rheological measurements are normally performed in kinematic instruments in order to get quantitative results useful for design and development of products and process equipment. A rheometric measurement normally consists of a strain (deformation) or a stress analysis at a constant frequency combined with a frequency analysis, e.g. between 0.1 and 100 Hz. The fluid samples are normally divided into three different groups according to their flow behavior.

(i) **Newtonian Fluid:** It is a fluid whose stress vs. strain rate curve remains linear. The constant of proportionality is called viscosity (η). Shear viscosity remains constant with shear rate.

(ii) **Non-Newtonian Fluids, Time Independent $\eta = \eta(\gamma)$**: In Non-Newtonian Fluids, time independent case, the viscosity of fluid is dependent on shear rate but independent of the time of shearing. The viscosity is presented at a specific shear rate and referred to as the "apparent viscosity", "shear viscosity" or "shear dependent viscosity". Shear-thinning (a decrease in viscosity with increasing shear rate, also referred to as Pseudoplasticity) and Shear-thickening (an increase in viscosity with increasing shear rate, also referred to as Dilatancy) are the two properties of Non-Newtonian, time independent fluid.

(iii) **Non-Newtonian Fluids, Time Dependent $\eta = \eta(\gamma,t)$**: In Non-Newtonian Fluids, time dependent case, the viscosity of fluid is dependent on shear rate and the time during which shear rate is applied. Thixotropy (a decrease in apparent viscosity with time under constant shear rate or shear stress, followed by a gradual recovery, when the stress or shear rate is removed) and Rheopexy (an increase in apparent viscosity with time under constant shear rate or shear stress, followed by a gradual recovery when the stress or shear rate is removed, also called anti-thixotropy or negative thixotropy) are the two properties of Non- Newtonian, time dependent fluids.

(b) **Oscillation Mode**

(i) **Frequency Sweep Measurement:** The material response to increasing frequency (rate of deformation) is monitored at a constant amplitude (stress or strain) and temperature. The frequency sweep gives information of the elastic modulus G', the viscous modulus G'' and the phase angle 'δ'. A large value of G' in comparison of G'' indicates pronounced elastic (gel) properties of the sample being analyzed. For such a product the phase angle is also small, e.g. 20° (a phase angle of 0° and 90° means a perfectly elastic and viscous material respectively) shown in Fig. 2.4.

The frequency sweep gives information about the gel strength where a large slope of the curve G' vs omega indicates low strength and a small slope indicates high strength. The stress in a dynamic experiment is referred to as the complex stress σ*. The complex stress can be separated into two components: an elastic stress in phase with the strain $\sigma' = \sigma^* \cos\delta$ (σ' is the degree to which material behaves like elastic solid) and

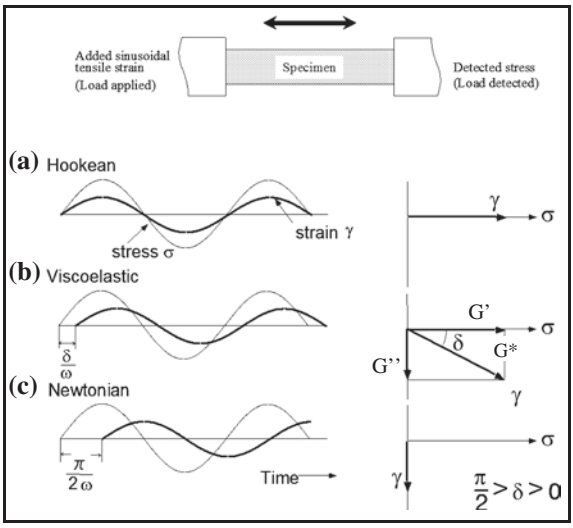

Fig. 2.4 Schematic picture of phase angle between stress (σ) and strain (γ) for **a** Hookean, **b** Viscoelastic and **c** Newtonian materials. Where G′ is real or storage modulus G″ is imaginary or loss modulus and G* is complex modulus

a viscous stress in phase with the strain rate $\sigma'' = \sigma^* \sin\delta$ (σ'' is the degree to which material behaves like a liquid). The complex modulus, $G^* = G' + iG''$ = (stress*/strain) is the measure of overall resistance to deformation. The elastic (storage) modulus, G' = (stress*/strain) cosδ is the measure of elasticity of the material, is the ability of material to store energy. The viscous (loss) modulus G'' = (stress*/strain) sinδ is the ability of the material to dissipate energy as heat. Tan delta ($\tan\delta = G''/G'$) is the measure of material damping-such as vibration or sound damping.

The viscosity measured in an oscillatory experiment is a complex viscosity much the way the modulus can be expressed as the complex modulus. The complex viscosity contains an elastic component and a term similar to the steady state viscosity. The complex viscosity is defined as: $\eta^* = \eta' - i\eta''$ or $\eta^*(\omega) = G^*/\omega = \sqrt{\left|G'(\omega)^2 + G''(\omega)^2\right|}\Big/\omega$. For viscoelastic gels, the complex viscosity is given by $|\eta*(\omega)| = \eta_0/\sqrt{1+\omega^2\tau_m^2}$ where, τ_m is the mean relaxation time for Maxwell model, η_0, the zero-shear viscosity related to the steady state viscosity and is the part of the measure of the rate of energy dissipation. Dynamic viscosity (η') for viscoelastic liquid approaches the steady flow viscosity (η_0) as the frequency approaches zero which is defined as $\eta' = G''/\omega$. The imaginary viscosity (η'') measures the elasticity or the stored energy and is related to the shear storage modulus which is defined as $\eta'' = G'/\omega$. The typical material response in a frequency sweep experiment is illustrated in Fig. 2.5.

(ii) **Temperature Sweep:** In our temperature sweep measurement, sample was loaded onto peltier plate of rheometer and allowed to equilibrate for 10 min. The periphery of geometry was coated with light silicon oil and enclosed by a wet sponge to minimize the solvent evaporation. Keeping the angular frequency fixed G' as a function of change in temperature of the peltier plate was recorded. The profile of G' versus temperature gives information about the thermal transition occurring in the material.

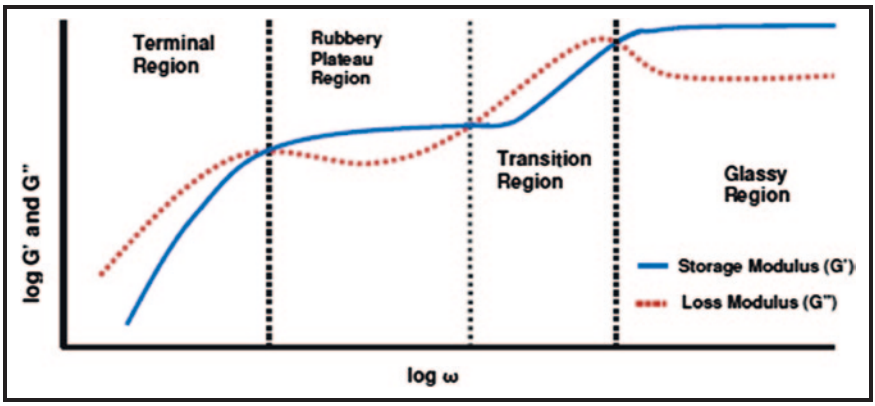

Fig. 2.5 The material response in a frequency sweep experiment

2.2.3 Viscometry

Viscosity measurements of nanoclay dispersions were performed on the Sine-wave Vibro (SV-10) Viscometer. SV-10 series has two thin plates as shown in Fig. 2.6. It drives with an ac frequency (30 Hz) by vibrating at constant sine-wave vibration in reverse phase like tuning fork. When the spring plates are vibrated with a same frequency, the amplitude varies in response to the amount of frictional force produced by the viscidity between the sensor plates and the sample.

To produce uniform amplitude, the vibro viscometer controls the electrical current that drives the vibration of the spring plates. Because the frictional force of viscidity is directly proportional to the viscosity, the driving electric current for vibrating the spring plates with a constant frequency to produce uniform amplitude is also directly proportional to the viscosity of each sample. The electromagnetic drive controls the vibration of the sensor plates to keep constant amplitude. The driving electric current which is the origin of exciting force, will be detected as the magnitude of the viscidity between the sensor plates and sample fluid. The vibro Viscometer measures the driving electric current, and then the viscosity is given by the positive correlation between the driving electric current and the viscosity. This resonating measuring and detection system has some advantage such as wide dynamic range and high resolution.

2.2.4 Tensiometry

Surface tension is a phenomenon in which the surface of a liquid, where the liquid is in contact with gas, acts like a thin elastic sheet. This term is typically used only when the liquid surface is in contact with gas (such as the air). If the surface is between two liquids such as water and oil, it is called interface. Energy is required

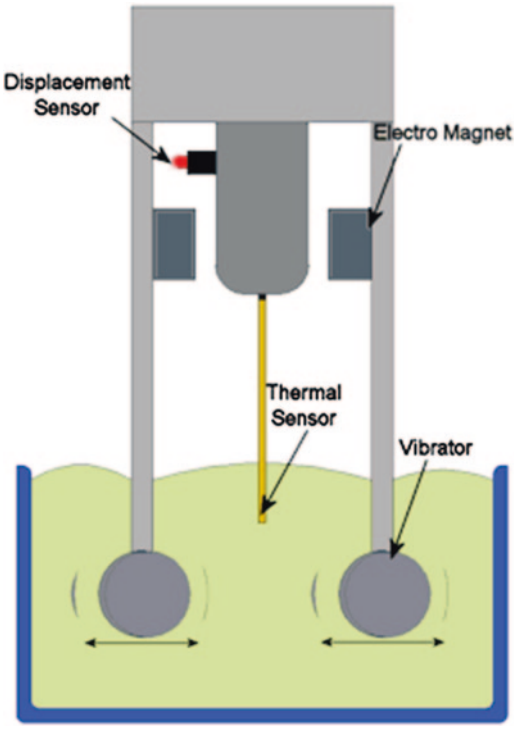

Fig. 2.6 Schematic of the vibro viscometer

to change the form of this surface or interface. The work required to change the shape of a given surface is known as the interfacial or surface tension. Surface tension (denoted with the Greek variable γ) is defined as the ratio of the surface force F to the length L along which the force acts; $\gamma = F/L$. In order to consider the thermodynamics of the situation, it is sometimes useful to consider it in terms of work per unit area.

Tensiometer is an instrument to measure the surface tension and/or interfacial tension of a liquid using the plate, ring or drop methods. It is a more difficult experimental measurement to accomplish and is not nearly as accurate as the plate method. In plate method, we require a plate to contact the liquid surface. It is widely considered the simplest and most accurate method for surface tension measurement. Most of the KRUSS tensiometers determine the surface tension with the help of an optimally wettable probe suspended from a precision balance; this is either a plate or a ring. A height-adjustable sample carrier is used to bring the liquid to be measured into contact with the probe. A force acts on the balance as soon as the probe touches the surface. If the length of the probe is known (circumference of ring or length of plate) the force measured can be used to calculate the interfacial or surface tension. A further requirement is that the probe must have a very high surface energy. This is why a platinum-iridium alloy is used for the

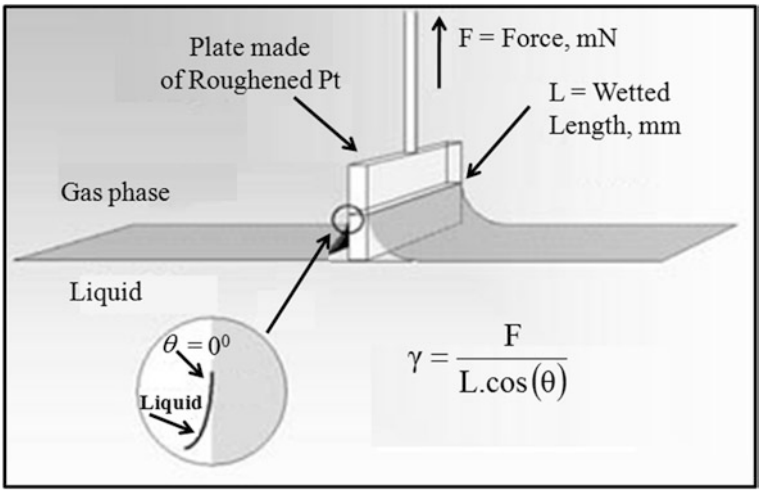

Fig. 2.7 Schematic of the plate method for measuring surface tension

ring and roughened platinum for the plate. In this work, K100MK2 KRUSS plate tensiometer, which is universal among tensiometer was used for surface tension measurement.

Figure 2.7 illustrates the schematic of plate method. In the plate method, the liquid is raised until the contact between the surface or interface, and the plate is established. Maximum tension acts on the balance at this instant; this means that the sample does not need to be moved again during the measurement. The tension is calculated using the following equation.

$$\gamma = \frac{F}{L \cdot \cos(\theta)} \tag{2.12}$$

where γ is surface tension; F is force acting on the balance; L is wetted length and θ is contact angle. The plate is made of roughened platinum and is optimally wetted so that the contact angle θ is virtually 0°. This means that the term cos θ has a value of approximately 1, so that only the measured force and the length of the plate need to be taken into consideration.

2.2.5 Electrophoresis

Electrophoresis is the phenomenon of the movement of a charged particle relative to the liquid suspended in, under the influence of an applied electric field [12–15]. The particle surface charge is one of the factors determining the physical stability of colloidal suspension and emulsions. Surface forces at the interface of

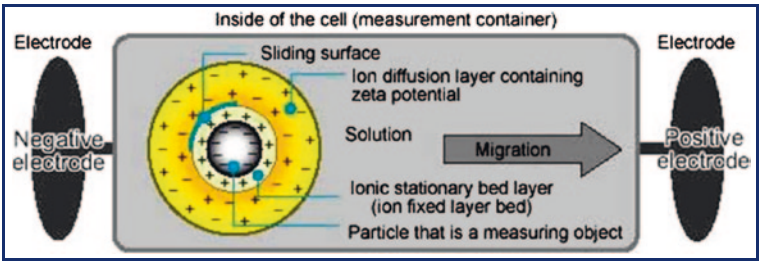

Fig. 2.8 The picture on the top shows a negatively charged molecule. Due to electrostatic attraction the counter ions make a layer around it to neutralize the interfacial potential, called stern layer or fixed layer and the ions with a small amount of the same polarity are distributed diffusely, called diffuse layer. (from Microtec Co., Ltd.)

the particle, and the liquid are very important because of the microscopic size of the colloids. Each colloid carries a like electrical charge which produces a force of mutual electrostatic repulsion between adjacent particles. Therefore, surface charge is a very good index of the magnitude of the interaction between colloidal particles, and this measurement is an important parameter to characterize colloidal dispersions. Typically, the particle charge is quantified as the so called zeta potential, which is measured e.g. via the electrophoretic mobility of the particles in an electric field. Alternatively the particle charge can be quantified in surface charge per surface unit, determined by colloid titration. It can be defined as the measure of overall charge, a particle acquires in a specific medium. In this thesis, the charge is characterized by the zeta potential.

The zeta potential theory is described in very detail by Müller in [11]. The development of a net charge at the particle surface affects the distribution of ions in the surrounding interfacial region, resulting in an increased concentration of counter ions (ions of opposite charge to that of the particle) close to the surface. Thus an electrical double layer exists around each particle as shown in Fig. 2.8. The liquid layer surrounding the particle exists as two parts; an inner region, called the Stern layer, where the ions are strongly bound and an outer, diffuse, region where they are less firmly attached. Within the diffuse layer there is a notional boundary inside which the ions and particles form a stable entity. When a particle moves (e.g. due to gravity), ions within the boundary move with it, but any ions beyond the boundary do not travel with the particle. This boundary is called the surface of hydrodynamic shear or slipping plane. The potential that exists at this boundary is known as the Zeta potential. That is to say, that the potential at the surface of shear of a charged particle i.e. for macro-ions it is the potential at the surface of the hydrodynamic particles. The conventional symbol used for zeta potential is "ζ" and it is usually measured in milli-volts (mV).

A zeta potential value quoted without a definition of its environment (pH, ionic strength, concentration of any additives) is a meaningless number. The

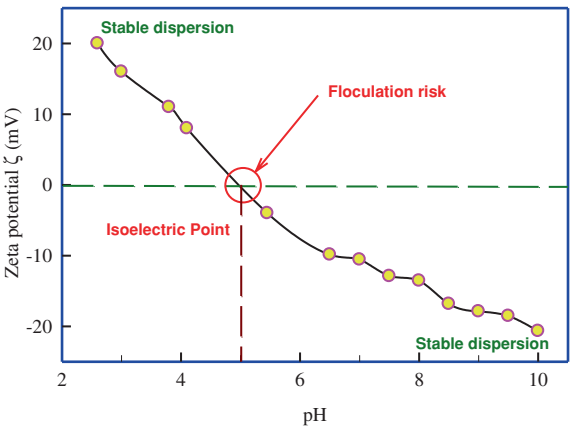

Fig. 2.9 Zeta potential of Gelatin B as function of pH. The system responds to pH by becoming more positively charged at lower pH (positive zeta potential) and more negatively charged at higher pH (negative zeta potential). At some intermediate pH, zeta potential is zero called the iso-electric point

magnitude of zeta potential gives an indication of the potential stability of the colloidal system. As the zeta rises, the repulsion between the particles becomes stronger. The stability of the dispersion gets higher while, on the other hand, as zeta approaches zero, the electrostatic build-up is relaxed allowing easier aggregation. A dividing line between the stable and unstable aqueous dispersion is generally taken at either $+30$ or -30 mV. Particles with zeta potentials more negative than -30 mV or more positive than $+30$ mV are normally considered stable (see Fig. 2.9). The most important factor that affects zeta potential is pH. The pH at which the net surface charge on the molecules became zero (or at which zeta potential becomes zero) is known as the isoelectric point of the solution. It is normally the point where the colloidal system is least stable. In general, a zeta potential versus pH curve will be positive at low pH and lower or negative at high pH.

We performed electrophoresis measurement on a zeta potential instrument (ZC-2000, Microtec, Japan). The sample solution is always necessary to dilute with dispersion medium (solvent). Dilution was done to isolate all individual particles from the aggregates and to know the distribution of charges on the surfaces of the single particle. In order to minimize the influence of electrolysis to the measurements, molybdenum $(+)$ and platinum $(-)$ plates were used as electrodes. Also, during the measurements, the cell chamber tap on molybdenum electrode was kept open to release the air bubbles, for reducing their effects on the particle movement. During the measurements, the molybdenum anode was cleaned each time as it turned from a metallic to blue-black color. The instrument was calibrated against 10^{-4} m AgI solution to meet the pre-measurement conditions set by the manufacturer. The nominal distribution of zeta potential is expected to be in the range -40 to -50 mV. To a good approximation, it can be presumed that zeta potential is directly proportional to the net charge on the particle if one assumes that the particles are non free-draining. Thus, the net surface charge density of the clusters becomes amenable.

2.2.6 Raman Spectroscopy

The energy of most molecular vibrations corresponds to the infrared region of the electromagnetic spectrum, and these vibrations may be detected in the range of few hundred to a few thousands cm^{-1} and measured in a Raman or infrared (IR) spectrum. Thus, Raman spectroscopy provides information about molecular vibrations that can be used for sample identification and quantitation. In Raman scattering measurements, a monochromatic light source, usually a single mode laser is incident on the sample and scattered light is detected. The majority of the scattered light is of the same frequency as the excitation source; this is known as Rayleigh or elastic scattering. Very small amount of the scattered light with lower (Stokes lines) or higher (Anti-Stokes lines) wavelength is shifted in frequencies from the laser frequency due to interactions between the incident electromagnetic waves, and the vibrational energy levels of the molecules in the sample. The energy difference between the incident and scattered light, so called Raman shift and usually expressed in terms of wave number $cm^{-1} = 1/\lambda$. This shift is independent of the frequency of the incident light. It is just a function of the properties of the scattering molecule. Using classical considerations the Stokes and Anti-Stokes lines should possess the same intensity but quantum-theoretical considerations show that the Raman effect is based on an inelastic photon scattering, which starts at the Stokes lines on a level with a small vibration quantum number and ends on a vibration level with a higher quantum number, whereas with the Anti-Stokes effect, the scattering process shows the inverse behavior.

When monochromatic light of frequency ν_P strikes a cell containing a transparent substance, most of the light passes through unaffected. However, some of the light is scattered by the sample in all directions. The scattered light contains photons having different frequencies from that of the incident light such as $(\nu_P - \nu_{vib})$ and $(\nu_P + \nu_{vib})$ and the same frequency ν_P as the incident light (elastic scattering). The difference corresponds to the energy change which has taken place within the molecule. The lines having lower frequency than the incident light $(\nu_P - \nu_{vib})$ are termed as Stokes lines (red shifted), while the high-frequency lines $(\nu_P + \nu_{vib})$ are termed as anti-Stokes lines (blue shifted). Figure 2.10 illustrates the energy level diagram in Raman scattering. For vibrational transitions, the anti-Stokes lines are usually weaker than the Stokes lines. In contrast to infrared spectroscopy, Raman spectroscopy is dependent on a change in the polarizability of a molecule during the vibration, and the intensity is related to the polarizability of the vibrating atoms, and their bonds present [14].

The water structure in clay dispersions were best probed by Raman spectroscopy as the Raman active vibrational modes are very sensitive to the local environment. The Raman spectra were recorded in back scattering configuration using a Renishaw Raman microscope with Ar-ion laser excitation at 514 nm. An incident maximum laser power of 50 mW was applied in order to avoid peak shifts due to thermal heating or structure transformations during data acquisition. We have also recorded Raman spectrum on a FT-IR/Raman Spectrometer with Microscope-Varian 7,000 FT-Raman with Ar-ion laser excitation at 1,064 nm and 450 mW power.

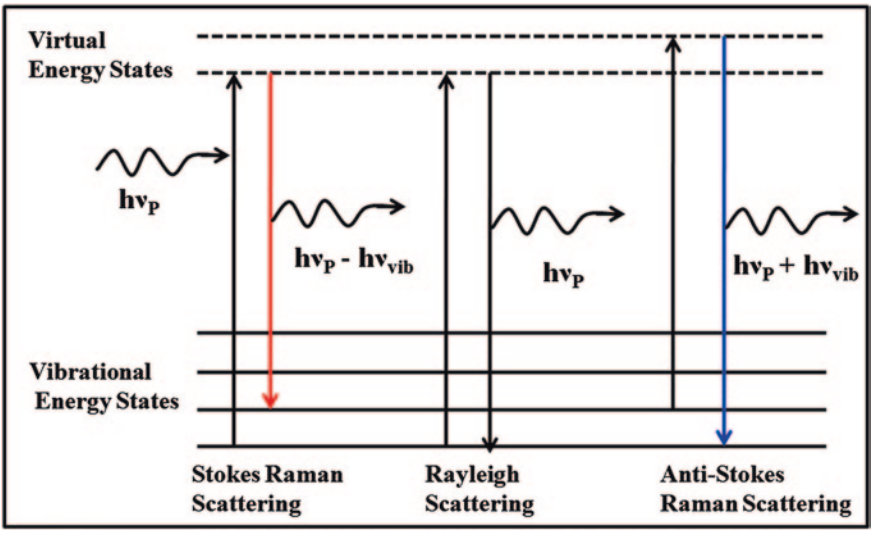

Fig. 2.10 Energy level diagram of states in Raman signal

2.2.7 Transmission Electron Microscopy

Transmission Electron Microscopy (TEM) is an imaging technique, uses a stream of monochromatic electrons that are focused to a small, thin, coherent beam by the use of condenser lenses. The wavelength of an electron is described by the de Broglie expression $\lambda = h/mv$, thus with suitable acceleration the desired angstrom wavelengths are achieved. In a transmission electron microscope (TEM), the ray of electrons is produced by a pin-shaped cathode heated up by current. The electrons are vacuumed up by a high voltage at the anode. The acceleration voltage is between 50 and 150 kV. The higher it is, the shorter are the electron waves, and the higher is the power of resolution. However, this factor is hardly ever limiting. The power of resolution of electron microscopy is usually restrained by the quality of the lens-systems and especially by the technique with which the preparation has been achieved. Modern gadgets have powers of resolution that range from 0.2 to 0.3 nm. The useful magnification is therefore, around 2,80,000×. The accelerated ray of electrons passes a drill-hole at the bottom of the anode. Its working principle is analogous to that of a ray of light in a light microscope. The lens-systems consist of electronic coils generating an electromagnetic field. The ray is first focused by a condenser. It then passes through the object, where it is partially deflected. The degree of deflection depends on the electron density of the object. The greater the mass of the atoms, the greater is the degree of deflection. After passing the object the scattered electrons are collected by an objective. Thereby, an image is formed, that is subsequently enlarged by an additional lens-system (called projective with electron microscopes). Thus formed image is made

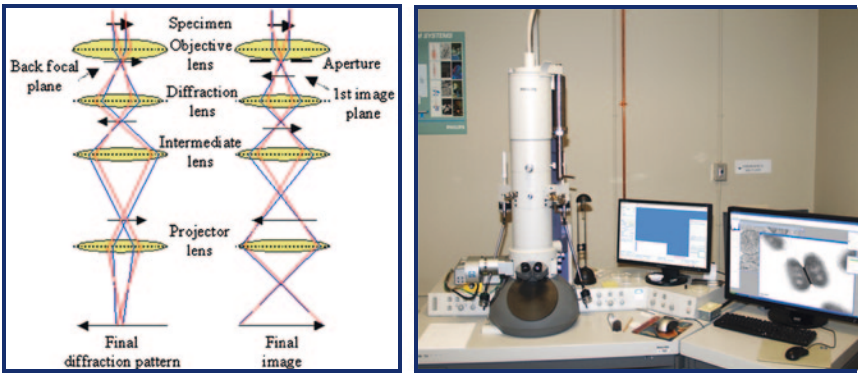

Fig. 2.11 Fei-Philips Morgagni 26&D transmission electron microscope used in the present work

visible on a fluorescent screen, or it is documented on photographic material. Photos taken with electron microscopes are in always black and white.

The TEM is an effective method to determine and/or verify the size and shape uniformity of nanoparticles within a sample, and used heavily in both material science/metallurgy and the biological sciences. In both cases, the specimens must be very thin and able to withstand the high vacuum present inside the instrument. In this work, the average particle size and morphology of clays were examined by Fei-Philips Morgagni 26&D transmission electron microscope (Digital TEM with image analysis system and Maximum Magnification = 2,80,000×) operating at a voltage of 100 kV (see Fig. 2.11). The aqueous dispersion of the clays was drop-cast onto a carbon coated copper grid and grid was air dried at room temperature (20 °C) before loading onto the microscope. In analytical TEMs the elemental composition of the specimen can be determined by analysing its X-ray spectrum or the energy-loss spectrum of the transmitted electrons. Modern research TEMs may include aberration correctors, to reduce the amount of distortions in the image, allowing information on features on the scale of 0.1 nm to be obtained (resolutions down to 0.08 nm has been demonstrated, so far). Monochromators may also be used, which reduce the energy spread of the incident electron beam to less than 0.15 eV.

2.2.8 X-Ray Diffraction

X-ray powder diffraction (XRD) is a convenient and powerful technique for materials investigation and was used for evaluating crystal structure and purities examination [1, 10]. For X-ray Diffraction (XRD) applications, the wavelength of X-rays roughly in the range between 0.01 and 10 nm (1–120 keV) are used. Because the wavelength of X-rays is comparable to the size of atoms, they are ideally suited for probing the structural arrangement of atoms and molecules in a wide range of materials [1, 10]. In X-rays diffraction experiment, an X-ray tube generates X-rays

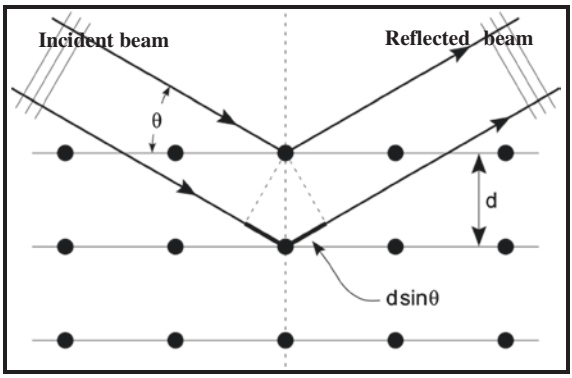

Fig. 2.12 Schematic of X-ray diffraction

by focusing an electron beam that has been accelerated across a high voltage field and bombards a stationary or rotating solid target. As electrons collide with atoms in the target and slow down, a continuous spectrum of X-rays are emitted, which are termed Bremsstrahlung radiation. The high energy electrons also eject inner shell electrons in atoms through the ionisation process. When a free electron fills the shell, an X-ray photon with energy characteristic of the target material is emitted. Two common targets are Mo and Cu, which have strong K_α X-ray emissions at 0.71073 and 1.5418 Å, respectively. W. L. Bragg found an simple geometrical interpretation $n\lambda = 2\ d \sin\theta$ (λ is the wavelength of incident waves which have an angle of incidence θ to a set of lattice planes at distance d, n is an integer), this equation making it easy to relate the angle of diffraction to the interplanar spacing and to allow us to make accurate quantification of the results of experiments carried out to determine crystal structure (see Fig. 2.12). In typical measurements, the diffractometer projects a beam of X-rays through the crystal. The diffracted beam is collimated through a narrow slit and passed through a nickel filter; in order to ensure that only one wavelength of X-rays reaches the counter.

In our work, the X-ray diffraction (XRD) measurements were recorded with a PANalytical X'Pert PRO diffractometer using a solid state detector with a monochromatized Cu $k_{\alpha 1}$ ($\lambda_{Cu} = 1.54060$ Å) radiation source at 45 kV. The powder sample was put on a powder holder. When the Bragg conditions for constructive interference are obtained, a "reflection" is produced, and the relative peak height is generally proportional to the number of grains in a preferred orientation. The x-ray spectra generated by this technique provide a structural finger-print of the unknown crystalline materials. Mostly, the diffraction data is used for phase identification. Each crystalline powder gives a unique diffraction diagram, which is the basis for a qualitative analysis by X-ray diffraction. Identification is practically always accompanied by the systematic comparison of the obtained spectrum with a standard one (a pattern), taken from any X-ray powder data file catalogues, published by the American Society for Testing and Materials (JCPDS). The diffraction profiles of a mixture of crystalline specimens consist in the spectra of each of the individual crystalline substances present, superposed. Thus, by examining the diffraction pattern, one can identify the crystalline phase of the material.

References

1. L.E. Alexander, *X-Ray Diffraction in Polymer Science* (Wiley, London, 1969)
2. H.A. Barnes, *A Handbook of Elementary Rheology* (University of Wales, Institute of Non-Newtonian fluid Mechanics, Aberystwyth, 2000)
3. G.B. Bendek, in *Thermal fluctuations and scattering of light; Lectures at Brandeis Summer Institute for Theoretical Physics* (1968)
4. B.J. Berne, R. Pecora, *Dynamic Light Scattering with Applications to Chemistry, Biology, and Physics* (Wiley Interscience, New York, 1976)
5. W. Burchard, in *Laser Light Scattering in Biochemistry*, ed. by S.E. Harding, D.B. Sattelle and V.A. Bloomfield (Royal Society of Chemistry, Cambridge, 1992)
6. W. Burchard, M. Schmidt, W.H. Stockmayer, Information on polydispersity and branching from combined quasi-elastic and intergrated scattering. Macromolecules **13**, 1265 (1980)
7. N.P. Cheremisinoff, P.N. Cheremisinoff, Introduction to Polymer Rheology and Processing. ISBN 13:9780849344022, CRC Press (1993)
8. B. Chu, *Laser Light Scattering* (Academic Press, New York, 1974)
9. T. Coviello, E. Geissler, D. Meier, Static and dynamic light scattering by a thermoreversible Gel from Rhizobium leguminosarum 8002 Exopolysaccharide. Macromolecules **30**, 2008 (1997)
10. H.P. Klug, L.E. Alexander, *X-Ray Diffraction Procedures for Polycrystalline and Amorphous Materials* (Wiley, New York, 1954)
11. R.H. Müller, Zetapotential und Partikelladung in der Laborpraxis—Einführung in die Theorie, praktische Meßdurchführung, Dateninterpretation, Wissenschaftliche Verlagsgesellschaft Stuttgart, 254 S (1996)
12. H. Ohshima, Electrostatic interaction between two spherical colloidal particles Adv. Coll. In. Sci. **53**, 77–102 (1994)
13. H. Ohshima, Electrophoresis of soft particles. Ad. Coll. In. Sci. **62**, 189–235 (1995)
14. B.P. Straughan, *Spectroscopy*, vol. 2. (Chapman & Hall, 1976). ISBN 0412133709, 9780412133701
15. M. von Smoluchowski, Versuch einer mathematischen theorie der Koagulationskinetik kolloidaler Lösungen. Z. Phys. Chem. **92**, 129–168 (1918)

http://www.springer.com/978-3-319-04554-2

Dispersion Stability, Microstructure and Phase Transition of Anisotropic Nanodiscs

Pujala, R.K.

2014, XVI, 154 p. 95 illus., 26 illus. in color., Hardcover
ISBN: 978-3-319-04554-2